Long-term Observation of the Soya Warm Current using HF Ocean Radars: Relationship between the Soya Warm Current variability and the sea level anomalies in the Soya/La Perouse Strait

Naoto Ebuchi[1, 2], Yasushi Fukamachi[3], Kay I. Ohshima[1, 2, 3], Humio Mitsudera[2], Jun Nishioka[2, 3], Toru Takatsuka[1], Kazuya Ono[1], Masao Ishikawa[1], Takaharu Daibo[1, 4], Kunio Shirasawa[2], Masaaki Wakatsuchi[1, 2]

1. Institute of Low Temperature Science, Hokkaido University
2. Pan-Okhotsk Research Center, Institute of Low Temperature Science, Hokkaido University
3. Arctic Research Center, Hokkaido University
4. Deceased

Revision 2 (May 07, 2024)

Corresponding author:
Naoto Ebuchi
Institute of Low Temperature Science, Hokkaido University
N19-W8, Kita-ku, Sapporo 060-0819, Japan
Phone: +81-11-706-5470, Fax: +81-11-706-7142
ebuchi@lowtem.hokudai.ac.jp
https://orcid.org/0000-0002-1069-5534

Abstract

Three High Frequency (HF) ocean radars were installed at the Soya/La Perouse Strait to monitor the surface current fields of the Soya Warm Current (SWC), which flows through the strait from the Sea of Japan to the Sea of Okhotsk. These ocean radars were operated for 19 years, from August 2003 to March 2022. In this paper, seasonal to interannual variations in the SWC were investigated using surface current fields obtained by the HF ocean radars combined with coastal tide gauge records and sea level anomaly from satellite altimetry. The HF ocean radars clearly captured the seasonal and interannual variations in the SWC. The alongshore surface velocity of SWC showed a high correlation with the alongshore sea level difference (SLD) between the Sea of Japan and the Sea of Okhotsk if seasonal variations were included. However, anomalies of the SLD and SWC alongshore velocity exhibited a lower correlation, especially in summer. This suggests that different mechanisms may be involved in summer and winter. The alongshore SLD between Wakkanai and Abashiri, which has been utilized in previous studies as an indicator of SWC intensity, may not be appropriate for representing interannual variations in the SWC intensity in summer, when the SWC reaches the maximum current velocity. Instead, it was demonstrated that the offshore SLD anomaly estimated using satellite altimetry with the coastal tide gauge record at Wakkanai could be a better index for representing the interannual variations throughout the year.

Keywords: HF ocean radar, Soya Warm Current, Soya/La Perouse Strait, Sea of Okhotsk, coastal boundary current

1. Introduction

The Soya Warm Current (SWC) flows from the Sea of Japan to the Sea of Okhotsk through the Soya/La Perouse Strait and is part of the Tsushima Warm Current System or the Japan Sea Through Flow (Kida et al., 2016, 2021). In the Sea of Okhotsk, the SWC flows along the coast of Hokkaido Island as a coastal boundary current (Hanawa, 1984). The SWC carries warm and saline water into the Sea of Okhotsk and affects oceanic and coastal environments. Based on field observations, previous studies (e.g., Aota, 1984; Aota and Matsuyama, 1987; Matsuyama et al., 1999, 2006) have revealed the structure, seasonal variations and driving mechanisms of the SWC. The dynamics of the SWC have been discussed in theoretical studies (e.g., Ohshima and Wakatsuchi, 1990; Ohshima, 1994; Mitsudera et al., 2011; Karaki et al., 2018). The SWC is ascribed to be driven by the sea level difference (SLD) between the Sea of Japan and the Sea of Okhotsk. The SLD between Wakkanai and Abashiri is commonly used to represent the SWC strength (Fig. 1).

Interannual variations in the SWC have not been revealed because long-term continuous observations have not been conducted due to difficulties in field observations. Geopolitical issues in the border strait and severe winter weather, including sea ice, have prevented research cruises across the strait. Because of the high fishing activity in this area, long-term observations using moored instruments are not possible. The barotropic structure of the SWC does not allow estimation of the geostrophic current from hydrographic observations and requires direct current measurements (e.g., Aota, 1984; Matsuyama et al., 1999, 2006). Frequent repeated observations are required because of the strong tidal current (mainly diurnal constituents) in and around the strait (e.g., Aota and Matsuyama, 1987; Odamaki, 1994).

To overcome these difficulties in in-situ measurements, High Frequency (HF) ocean radars (e.g., Barrick et al., 1977; Prandle, 1991) were installed around the Soya Strait, and continuous observations of the surface current vectors over the strait were conducted for 19 years, from August 2003 to March 2022. Ebuchi et al. (2006) compared the surface current velocity measured by the HF ocean radars with in-situ measurements using drifting buoys and shipboard Acoustic Doppler Current Profiles (ADCPs) and confirmed reasonable agreement. Analyzing the HF ocean radar data, they also described the tidal currents in this region and seasonal and short-term variations in the SWC. Ebuchi et al. (2009) investigated the subinertial variations in the SWC using data obtained from the HF ocean radars, coastal tide gauges, and a bottom-mounted ADCP. Fukamachi et al. (2008, 2010) estimated the volume transport of SWC by combining surface velocity fields from the HF ocean radars and vertical velocity profiles from bottom-mounted ADCPs. Ohshima et al. (2017) and Ohshima and Kuga (2023) attempted to compose a long-term time series of SWC volume transport by combining data from the HF ocean radars, historical hydrographic observations, and tide gauge records.

The objective of this paper is to clarify the seasonal to interannual variations in the SWC and provide information to discuss dynamics of the SWC through relationships with coastal sea level variations. We analyzed the surface current velocity fields over 19 years obtained by the HF ocean radars around the Soya Strait, together with tide gauge records and sea level data from satellite altimetry and discussed seasonal to interannual variations in the SWC. Section 2 describes the data used in this paper and data processing. The results and discussion are presented in Section 3. Section 4 presents a summary and concluding remarks.

2. Data and data processing

2.1. HF ocean radars

In 2003, the Institute of Low Temperature Science, Hokkaido University, installed three HF ocean radar stations around the Soya Strait. Continuous monitoring of the surface current field of SWC was started in August 2003. The locations of the stations are shown in Fig. 1 (solid circles with NS, SY, and SR labels). The installed HF ocean radars were SeaSonde systems manufactured by CODAR, Ltd. The central frequency is 13.9 MHz. Each radar station covered approximately 70 km from the station, with range and azimuth resolutions of 3 km and 5°, respectively. The radar measured the radial components of the surface current velocity as temporal averages over a period of 1 hour. By combining the radial velocity components measured at the three stations, the surface current vectors were composed using the least squares method on 3-km grids (dots in Fig. 1). Details of the radars, stations, and data processing are described by Ebuchi et al. (2006). Operation of the HF ocean radar stations was terminated in March 2022. We obtained a long-term continuous record of the SWC surface current field over 19 years, with several gaps spanning hours to months, due to various issues during observations.

Ebuchi et al. (2006) compared surface current vectors derived from the HF ocean radars with measurements from surface drifting buoys and shipboard ADCPs (Acoustic Doppler Current Profilers). It was confirmed that the surface current velocity measured by the HF ocean radars agreed well with the in-situ measurements. The typical root-mean-square error was approximately 20 cm s^{-1}. Fukamachi et al. (2008, 2010) found a similar agreement with measurements using bottom-mounted ADCPs.

We analyzed hourly surface current vector data observed by the HF ocean radars from August 2003 to March 2022. To remove the tidal components, a 25-hour running average was applied to the hourly time series, and the daily vector-average current fields were composed. Wind drift components were removed using the method proposed by Zhang et al. (2016) with the GPV/MSM (Grid Point Values/Moso-Scale Model) surface wind field data from the Japan Meteorological

Agency (JMA). The monthly vector-average surface current fields were calculated from the daily mean field.

2.2 Coastal sea level data

Because the SWC is ascribed to be driven by the SLD between the Sea of Japan and the Sea of Okhotsk (Ohshima and Wakatsuchi, 1990; Ohshima, 1994), the SLD between the Wakkanai (WK in Fig. 1) and Abashiri (AB in Fig. 1) tide gauge stations has been commonly utilized to represent the strength of the SWC in previous studies (e.g., Aota, 1984, 1987). We obtained hourly tide gauge records from the two stations. A 48-hour tide killer filter developed by Hanawa and Mitsudera (1985) was applied to remove tidal constituents, and daily mean sea levels were calculated. Static atmospheric pressure correction was applied using the daily mean sea level pressure data obtained at weather stations in Wakkanai and Abashiri.

To discuss long-term variations in sea level based on tide gauge records, we must consider land movement. Figure 2 shows the vertical land displacement anomalies observed at the GPS stations operated by the Geological Survey, Japan. We used data from the Wakkanai and Shari GPS stations (WK and SH in Fig. 1), because operation of the Abashiri GPS station was started in 2014. The distance between the two stations is approximately 55 km. We confirmed that the vertical land displacements at Abashiri and Shari agreed very well for the period from 2014 to 2022.

From 2003 to 2022, both stations rose continuously. However, the difference between the two stations remained almost constant before 2011 and began to decrease after 2011. The magnitude of variation during this period was approximately 3 cm. We applied a 13-month running average to remove short-term variations, and used it to correct for the effects of land motion in the sea level.

2.3. Satellite altimetry data

Along-track sea level anomaly (SLA) data from the TOPEX/POSEIDON and Jason-1, -2, and -3 satellite altimeters were used to represent the offshore sea level. We utilized the data products of delayed-time, mono-mission, along-track SLA provided by the Archiving, Validation, and Interpretation of Satellite Oceanographic Data (AVISO)/Altimetry. The data products were downloaded from the Copernicus Marine Data Store. As shown in Fig. 1, Track 025 passes across the coverage of the HF ocean radars. The temporal interval of the observations was 9.91 days and the spatial resolution along the track was 6.7 km. Because the altimeters cannot measure the SLA accurately in the coastal region, we attempted to estimate anomalies of the SLD across the SWC by combining the altimeter-derived offshore SLA and tide gauge records at the Wakkanai Station.

3. Results and discussion

Figure 3 shows the monthly variations in the observed surface current vector fields. The monthly mean current vectors were averaged over the entire observation period for each month. The SWC flows along the coast of Hokkaido and exhibits clear seasonal variations. It was strong in summer and weak in winter. The current velocity increases downstream of the Soya Strait.

The magnitude of the alongshore velocity component across Line A (Figs. 1 and 3) is shown as a function of distance from the coast in Fig. 4. Line A was selected because the alongshore velocity was the strongest, and data acquisition rate was the highest in the observation area. The thin blue lines indicate the horizontal profile of alongshore velocity for each year. The thick red lines with error bars indicate the average and standard deviations over the entire observation period. It is clear that almost the same seasonal cycle was repeated during this period, although interannual variations in the strength and current axis location of SWC were also discernible. In summer, the axis of the

SWC is located 20-30 km from the coast, and the maximum velocity is 0.8-1.0 m s^{-1}. In winter, the SWC almost disappeared from the surface current profile (see also Fig. 3).

The alongshore current velocity was averaged in Box B, as indicated in Figs. 1 and 3, which is approximately located at the axis of the SWC and expands from 20 to 40 km offshore and 15 x 15 km in the zonal and meridional directions. The time series is shown in Fig. 5, along with the alongshore SLD between Wakkanai and Abashiri. As demonstrated in previous studies (e.g., Aota, 1984; Aota and Matsuyama, 1987; Ebuchi et al. 2006, 2009), the two time series showed good correlation with a correlation coefficient of 0.871 because they exhibited distinct seasonal variations.

Figure 6 shows the seasonal variations averaged over the entire observation period together with the standard deviations in the 19 years. Although the alongshore velocity and alongshore SLD varied in phase, a broader summer peak was discernible in the SLD than in the alongshore velocity. Seasonal variations were dominant in the two long-term time series, resulting in a high correlation between them, as shown in Fig. 5.

Anomalies were calculated from the two time series shown in Fig. 5 by subtracting the mean seasonal variation shown in Fig. 6. The results are shown in Fig. 7. The correlation coefficient was 0.584. Some peaks coincided in the two time series, whereas others did not. Variations at the decadal scale, including a recent increasing trend in the SWC, were also discernible in both the velocity and SLD anomalies. The amplitude of this trend was approximately 5 cm. This implies that the difference in vertical land displacements shown in Fig. 2 is not negligible, and a correction for land displacement is needed to investigate long-term variations in the coastal tide gauge records.

Scatter plots of the two time series with (Fig. 5) and without (Fig. 7) seasonal variations are shown in Fig. 8. The differences in the correlations are shown in Fig. 8. The correlation coefficient between the anomalies of the alongshore current velocity in Box B and the alongshore sea level difference between Wakkanai and Abashiri was calculated for each month. The slope of regression line was also calculated by the Principal Component Analysis (PCA). The results are shown in Fig. 9. The correlation coefficient was high in the winter and low in the summer, although some fluctuations were observed. The slope also exhibited seasonal variation in concert with the correlation coefficient. Especially data from August to October showed higher values of the slope.

In Fig. 8(b), the number of data points, correlation coefficients, and slope calculated by the PCA though a year are 215, 0.584, and 3.34 cm s^{-1}/cm, respectively. In Fig. 8, blue dots, red open circles and red dots indicate data obtained in winter (November-April) and summer (May-July, and August-October), respectively. In Fig. 8(b), the anomalies of the alongshore SLD and the alongshore velocity of the SWC correlated better in winter than in summer, especially in August-October, as shown in Fig. 9. The correlation coefficients are 0.750 and 0.411, and the slope calculated by the PCA are 3.59 and 9.34 cm s^{-1}/cm for winter and summer, respectively. In Fig. 8(a), a good linear relationship between the alongshore SLD and alongshore velocity is discernible in the lower range of these parameters, which corresponds to the winter data (blue dots). In summer (red dots and red open circles, higher alongshore SLD and alongshore velocity), the velocity did not seem to correlate well with the SLD. This result is consistent with that reported by Ohshima et al. (2017) for the volume transport of SWC.

These results suggest that different mechanisms work in the generation and maintenance of SWC in winter and summer. Fukamachi et al. (2008, their Fig. 2) and Fukamachi et al. (2010, their Fig. 4) exhibited seasonal variations in the SWC vertical velocity profile. In winter, the SWC shows a barotropic structure, and the SLD between the Sea of Japan and Sea of Okhotsk is directly related to the strength of the surface current. The SLD is considered to be governed by sea level in the Sea of Okhotsk, which is largely affected by wind-generated arrested topography waves (Csanady, 1978), as already reported in previous studies (e.g., Simizu and Ohshima, 2006; Ohshima et al., 2017; Tsujino et al., 2008; Kida et al., 2016, 2021). In summer, the SWC becomes more baroclinic, and vertical stratification may affect the vertical structure of SWC. This may reduce the correlation between the SLD and surface current velocity. The results shown in Figs. 8 and 9 is in concert with the seasonal variations in the vertical velocity structure of the SWC, as observed by Fukamachi et al. (2008, 2010). According to the results, the alongshore SLD between Wakkanai and Abashiri may not be a good indicator of the strength of SWC in summer on interannual time scales, although it has been used conventionally.

In the offshore direction, the geostrophic balance between the Coriolis force and the pressure gradient is considered to hold in the SWC. In this balance, the alongshore surface current velocity should be proportional to the offshore SLD, which is an ideal indicator of the strength of SWC. To estimate the offshore SLD, we required a tide gauge record from a station on Sakhalin Island, which is currently very difficult to obtain. Instead, in this study, we attempted to estimate the offshore SLD anomaly using satellite altimetry.

As shown in Fig. 1, the ground track 025 of the TOPEX/POSEIDON, Jason-1, -2, and -3 altimeters passing the observation are of the HF ocean radars. However, satellite altimeters cannot accurately measure the sea surface height near the coast. Therefore, we used the offshore SLA derived from satellite altimetry with coastal tide gauge data from Wakkanai. The altimeter-derived SLA was averaged at latitude between 45.66° N and 46.00° N. The instantaneous values observed in each cycle with a temporal interval of 9.91 days were utilized without any temporal smoothing. The daily mean value of the coastal sea level at Wakkanai was used to estimate the offshore SLD anomaly. Daily mean alongshore velocity was used for comparison. Please note the difference of the temporal averaging scale with the results shown in Figs. 8 and 9.

Figure 10(a) shows a scatter plot of the offshore SLD anomaly from the average over the entire period and the HF alongshore surface velocity. The number of data, correlation coefficient, slope calculated by the PCA were 474, 0.842, 3.25 cm s^{-1}/cm, respectively. Anomalies from the mean seasonal variation are plotted in Fig. 10(b). The correlation coefficient and slope throughout the year were 0.620 and 5.03 cm s^{-1}/cm, respectively. As expected, the offshore SLA exhibited a good correlation with the alongshore surface current velocity in panels (a) and (b), indicating the geostrophic balance in the SWC. Assuming the geostrophic balance between the sea level difference across the SWC, Δh, and the mean surface velocity, U, the slope is expressed as,

$$U/\Delta h = g/f\,L, \quad (1)$$

where g is the acceleration of gravity, f is the Coriolis parameter, and L is the horizontal distance across the SWC. Substituting g = 9.8 m s^{-2}, f = 10^{-4} s^{-1}, and L = 40 km (see Fig. 4), $U/\Delta h$ is roughly estimated to be 2.5 s^{-1}, which is consistent with the value obtained above, if we consider that the surface velocity plotted in Fig.10 was observed at the SWC axis and is higher than the mean velocity, U.

In Fig. 10, data obtained in winter and summer are indicated by blue and red dots, as in Fig. 8. In Fig. 10(a), the data in summer and winter exhibit consistent relationship between the SWC velocity and the offshore SLD anomaly. In Fig. 10(b), the correlation coefficients were 0.683 and 0.564, and the slope were 5.00 and 5.05 cm s^{-1}/cm in winter and summer, respectively. The difference between winter and summer was much lower than that shown in Fig. 8(b). The geostrophic balance between the offshore SLD and the alongshore surface current velocity should be maintained regardless of vertical stratification in both winter and summer.

4. Summary and concluding remarks

We operated the HF ocean radars around the Soya Strait for 19 years, from August 2003 to March 2022. In this paper, seasonal to interannual variabilities in the SWC are discussed using the data together with coastal tide gauge records and SLA from satellite altimetry. The HF ocean radars clearly captured the seasonal and interannual variations in the SWC. The alongshore surface velocity of SWC showed a high correlation with the alongshore SLD between Wakkanai and Abashiri, if seasonal variations were included. However, anomalies from the mean seasonal variations of the alongshore SLD and alongshore current velocity of SWC exhibited a lower correlation, especially in summer. This suggests that different mechanisms may be involved in summer and winter. The alongshore SLD between Wakkanai and Abashiri, which has been used in previous studies, may not be appropriate for representing interannual variations in the SWC in summer, when the SWC reached the maximum velocity. Instead, the offshore SLD anomaly estimated using satellite altimetry with the coastal tide gauge record at Wakkanai could be a better index for representing interannual variations in both winter and summer.

The SWC is considered to be driven by the SLD between the Sea of Japan and the Sea of Okhotsk (e.g., Ohshima and Wakatsuchi, 1990; Ohshima, 1994). It is conjectured that the pressure gradient due to the SLD is balanced by the bottom friction. However, judging from the vertical structure of the SWC velocity (e.g., Fukamachi et al., 2008, 2010), the effects of bottom friction on the vertical structure of the SWC do not seem simple. Although new theoretical studies on the structure of SWC have been performed by Mitsudera et al. (2011) and Karaki et al. (2018), further studies are required to reveal the detailed dynamic mechanisms of the formation, maintenance, and fluctuation of the SWC. The results suggest that vertical stratification plays an important role. Ohshima and Kuga (2023) attempted to develop a new method to estimate the SWC volume transport from the alongshore SLD between Wakkanai and Abashiri by explicitly considering the baroclinic component.

In this study, we utilized standard altimeter SLA data product to estimate the offshore SLD combined with the coastal sea level at the Wakkanai tide gauge station because standard altimeter data do not contain accurate SLA in coastal regions. However, prototype coastal altimeter products, such as PISTACH (Prototype Innovant de Système de Traitement pour les Applications Côtières et l'Hydrologie) and CTOH (Center for Topographic Studies of the Oceans and Hydrosphere), have recently been produced and distributed by several research projects (e.g., Vignudelli et al., 2011). Although it is not straightforward to use these coastal altimeter products compared to the standard altimeter products at present, we may directly derive the SLA profiles of the SWC in the coastal region from these data products in future studies. In December 2022, a new type of satellite altimeter, the Ka-band Radar Interferometer (KaRIN) on Surface water and Ocean Topography (SWOT) satellite, was launched by the National Aeronautics and Space Administration (NASA). It measures ocean and surface water levels over a 120-km wide swath with a 20 km gap along the nadir. The typical spatial resolution of the SLA measurements is 1 km. Using this new type of satellite altimeter, we can observe more detailed features of the SWC.

Acknowledgments

We would like to thank Akira Masuda, Kenji Marubayashi, Michiyoshi Ishibashi, and Kei Yufu of the Research Institute for Applied Mechanics (RIAM) of Kyushu University; Satoshi Fujii of University of the Ryukyus; Akitsugu Nadai of the National Institute of Information and

Communications Technology for their advice regarding the design, construction, operation, and data analyses of the HF ocean radar system. Discussions during the research workshops hosted by the RIAM and the Institute of Low Temperature Science (ILTS) of Hokkaido University under their Joint/Use Research Programs were very helpful during the course of this study. Thanks are also extended to the Hokkaido Bureau of Telecommunications of the Ministry of Internal Affairs and Communications, the Wakkanai and Abashiri Construction Management Departments of the Hokkaido Government, Wakkanai City, Mombetsu City, the Hokkaido Wakkanai Fisheries Experimental Station, the Soya Fisheries Cooperative Association, and the technicians and administrative staffs of the ILTS for their contributions and cooperation with the construction, maintenance, and operation of the HF ocean radar stations.

The surface current data from the HF ocean radars analyzed in this study are available to scientific research users through the Joint/Use Research Program hosted by the Institute of Low Temperature Science, Hokkaido University. Please contact hfradar@lowtem.hokudai.ac.jp.

The tide gauge records and sea level pressure data used in this paper were downloaded from the website of the Japan Meteorological Agency. The JMA GPV-MSM data were downloaded from the website of the Research Institute of Sustainable Humanosphere, Kyoto University. The GPS data were downloaded from the website of the Geographical Survey, Japan. The altimetry data produced by AVISO/Altimetry were downloaded from the Copernicus Marine Data Store website. Most figures in this paper were produced using the GFD-DENNOU Library. The present study was financially supported in part by the JSPS KAKENHI Grant Numbers 16H02226 and 21K12204, and the Pan-Okhotsk Research Center of ILTS.

References

Aota, M., 1984: Oceanographic structure of the Soya Warm Current. *Bull. Coast. Oceanogr.*, **22**(1), 30-39 (in Japanese). https://doi.org/10.32142/engankaiyo.22.1_30

Aota, M., and M. Matsuyama, 1987: Tidal current fluctuations in the Soya Current. *J. Oceanogr. Soc. Jpn*, **43**(5), 276-282. https://doi.org/10.1007/BF02108695

Barrick, D. E., M. W. Evans, and B. L. Weber, 1977: Ocean surface currents mapped by radar. *Science*, **198**, 138-144. https://doi.org/10.1126/science.198.4313.138

Csanady, G. T., 1978: The arrested topographic wave. *J. Phys. Oceanogr.*, **8**, 47-62. https://doi:10.1175/1520-0485(1978)008,0047:TATW.2.0.CO;2

Ebuchi, N., Y. Fukamachi, K.I. Ohshima, K. Shirasawa, M. Ishikawa, T. Takatsuka, T. Daibo, and M. Wakatsuchi, 2006: Observation of the Soya Warm Current using HF radar. *J. Oceanogr.*, **62**(1), 47-61. https://doi.org/10.1007/s10872-006-0031-0

Ebuchi, N., Y. Fukamachi, K.I. Ohshima, and M. Wakatsuchi, 2009: Subinertial, and seasonal and variations in the Soya Warm Current revealed by HF radars, coastal tide gauges, and a bottom-mounted ADCP. *J. Oceanogr.*, **65**(1), 31-43. https://doi.org/10.1007/s10872-009-0003-2

Fukamachi, Y. I. Tanaka, K.I. Ohshima, N. Ebuchi, G. Mizuta, H. Yoshida, S. Takayanagi, and M. Wakatsuchi, 2008: Volume transport of the Soya Warm Current revealed by bottom-mounted ADCP and ocean-radar measurement. *J. Oceanogr.*, **64**(3), 385-392. https://doi.org/10.1007/s10872-008-0031-3

Fukamachi, Y., K. I. Ohshima, N. Ebuchi, T. Bando, K. Ono, and M. Sano, 2010: Volume transport in the Soya Strait during 2006-2008. *J. Oceanogr.*, **66**(5), 685-696. https://doi.org/10.1007/s10872-010-0056-2

Hanawa, K., 1984: Coastal Boundary Current. *Bull. Coast. Oceanogr.*, **22**(1), 67-82 (in Japanese). https://doi.org/10.32142/engankaiyo.22.1_67

Hanawa, K., and H. Mitsudera, 1985: On the data processing of daily mean values of oceanographic data—Note on the daily mean sea-level data—. *Bull. Coast. Oceanogr.*, **23**, 79–87 (in Japanese). https://doi.org/10.32142/engankaiyo.22.1_67

Karaki, T., H. Mitsudera, and H. Kuroda, 2018: Buoyancy shutdown process for the development of the baroclinic jet structure of the Soya Warm Current during summer. *J. Oceanogr.*, **74**, 339–350. https://doi.org/10.1007/s10872-018-0465-1

Kida, S., B. Qiu, J. Yang, and X. Lin, 2016: The annual cycle of the Japan Sea Throughflow. *J. Phys. Oceanogr.*, **46**, 23–39. https://doi.org/10.1175/JPO-D-15-0075.1

Kida, S., K. Takayama, Y. N. Sasaki, H. Matsuura, and N. Hirose, 2021: Increasing trend in Japan Sea Throughflow transport. *J. Oceanogr.*, **77**(1), 145–153. https://doi.org/10.1007/s10872-020-00563-5

Matsuyama, M., M. Aota, I. Ogasawara, and S. Matsuyama, 1999: Seasonal variation of Soya Current. *Umi no Kenkyu (Oceanography in Japan)*, **8**, 333–338 (in Japanese). https://doi.org/10.5928/kaiyou.8.333

Matsuyama, M., M. Wadaka, T. Abe, M. Aota and Y. Koike, 2006: Current structure and volume transport of the Soya Warm Current in summer. *J. Oceanogr.*, **62**(2), 197–205. https://doi.org/10.1007/s10872-006-0044-8

Mitsudera, H., K. Uchimoto, and T. Nakamura, 2011: Rotating stratified barotropic flow over topography: mechanisms of the cold belt formation off the Soya Warm Current along the northeastern coast of Hokkaido. *J. Phys. Oceanogr.*, **41**(11), 2120–2136. https://doi.org/10.1175/2011JPO4598.1

Odamaki, M., 1994: Tides and tidal currents along the Okhotsk coast of Hokkaido. *J. Oceanogr.*, **50**(3), 265–279. https://doi.org/10.1007/BF02239517

Ohshima, K. I. and M. Wakatsuchi, 1990: A numerical study of barotropic instability associated with the Soya Warm Current in the Sea of Okhotsk. *J. Phys. Oceanogr.*, **20**(4), 570-584. https://doi.org/10.1175/1520-0485(1990)020<0570:ANSOBI>2.0.CO;2

Ohshima, K.I., 1994: The flow system in the Sea of Japan caused by a sea level difference through shallow straits. *J. Geophys. Res.*, **99**(C5), 9925–9940. https://doi.org/10.1029/94JC00170

Ohshima, K. I., D. Simizu, N. Ebuchi, S. Morishima, and H. Kashiwase, 2017: Volume, heat, and salt transports through the Soya Strait and their seasonal and interannual variations. *J. Phys. Oceanogr.*, **47**(5), 999-1019. https://doi.org/10.1175/JPO-D-16-0210.1

Ohshima, K.I., and M. Kuga, 2023: 50-year volume transport of the Soya Warm Current estimated from the sea-level difference and its relationship with the Tsushima and Tsugaru Warm Currents. *J Oceanogr.* **79**(5), 499-515. https://doi.org/10.1007/s10872-023-00693-6

Prandle, D., 1991: A new view of near-shore dynamics based on observations from HF radar. *Prog. Oceanogr.*, **27**(3-4), 403-438. https://doi.org/10.1016/0079-6611(91)90030-P

Simizu, D., and K. I. Ohshima, 2006: A model simulation on the circulation in the Sea of Okhotsk and the East Sakhalin Current. *J. Geophys. Res.*, **111**, C05016. https://doi.org/10.1029/2005JC002980

Tsujino, H., H. Nakano and T. Motoi, 2008: Mechanism of currents through the straits of the Japan Sea: mean state and seasonal variation. *J. Oceanogr.*, **64**(1), 141–161. https://doi.org/10.1007/s10872-008-0011-7

Vignudelli, S., A. G. Kostianoy, P. Cipollini, and Jérôme Benveniste (eds), 2011: Coastal Altimetry. Springer Science & Business Media, pp. 566.

Zhang, W., N. Ebuchi, Y. Fukamachi, Y. Yoshikawa, 2016: Estimation of wind drift current in the Soya Strait. *J. Oceanogr.*, **72**(2), 299-311. https://doi.org/10.1007/s10872-015-0333-1

Figure legends

Figure 1. Map of the Soya/La Perouse Strait, location and coverage of the HF radar stations (solid circles, NS: Noshappu radar station, SY: Soya radar station, SR: Sarufutsu radar station), locations of the tide gauge stations (solid triangles, WK: Wakkanai, AB: Abashiri), and GPS stations (solid squares, WK: Wakkanai, SH: Shari). Fans indicate 70 km radii from the HF ocean radar stations and approximate directions of observations. The dots are 3-km grids, where the surface current vectors are composed from the radial velocity components obtained at the HF ocean radar stations. Line A and Box B were used to depict the horizontal alongshore velocity profiles and estimate the alongshore velocity at the SWC axis, respectively. The thin line labeled 025 indicates ground track 025 of satellite altimetry (TOPEX/POSEIODON, Jason-1, -2, and -3).

Figure 2. Anomalies of vertical land movements at the GPS stations in Wakkanai (red) and Shari (blue), and the difference between the two stations (black). The average values for the entire study period were subtracted.

Figure 3. Bi-monthly variations in monthly mean surface current fields. (a) February, (b) April, (c) June, (d) August, (e) October, and (f) December. The locations of Line A and Box B are indicated by red line and blue box. Monthly maps for the full 12 months are shown in Online Resource 1.

Figure 4. Magnitude of the alongshore velocity component along Line A (Fig. 1) as a function of distance from the coast. The thin blue lines indicate the monthly mean horizontal profile of

the alongshore velocity for each year. The thick red lines with error bars indicate the average and standard deviations over the entire observation period.

Figure 5. Time series of monthly mean alongshore current velocity in Box B (blue) and alongshore sea level difference between Wakkanai and Abashiri (red).

Figure 6. Seasonal variations in the alongshore current velocity in Box B (blue) and the alongshore sea level difference between Wakkanai and Abashiri (red) averaged over the entire observation period. Error bars indicate the standard deviations.

Figure 7. Anomalies of the alongshore current velocity in Box B (blue) and the alongshore sea level difference between Wakkanai and Abashiri (red) from the mean monthly average over the entire observation period.

Figure 8. Scatter plots of the alongshore current velocity in Box B and the alongshore sea level difference between Wakkanai and Abashiri (a) with and (b) without seasonal variation. Red open circles, red dots and blue dots indicate the data obtained in May-July, August-October, and November-April, respectively.

Figure 9. Seasonal variations in the correlation coefficient between the anomalies of the alongshore current velocity in Box B and the alongshore sea level difference between Wakkanai and Abashiri from the mean monthly average over the entire observation period (red). Slopes calculated from the PCA analysis is indicated in blue.

Figure 10. Scatter plots of the offshore sea level difference anomaly estimated using satellite altimetry and coastal tide gauge records at Wakkanai and the HF alongshore surface velocity. (a) Absolute values including seasonal variations, and (b) anomalies from the mean monthly average over the entire observation period. Red and blue dots indicate the data obtained in summer (May-October) and winter (November-April), respectively.

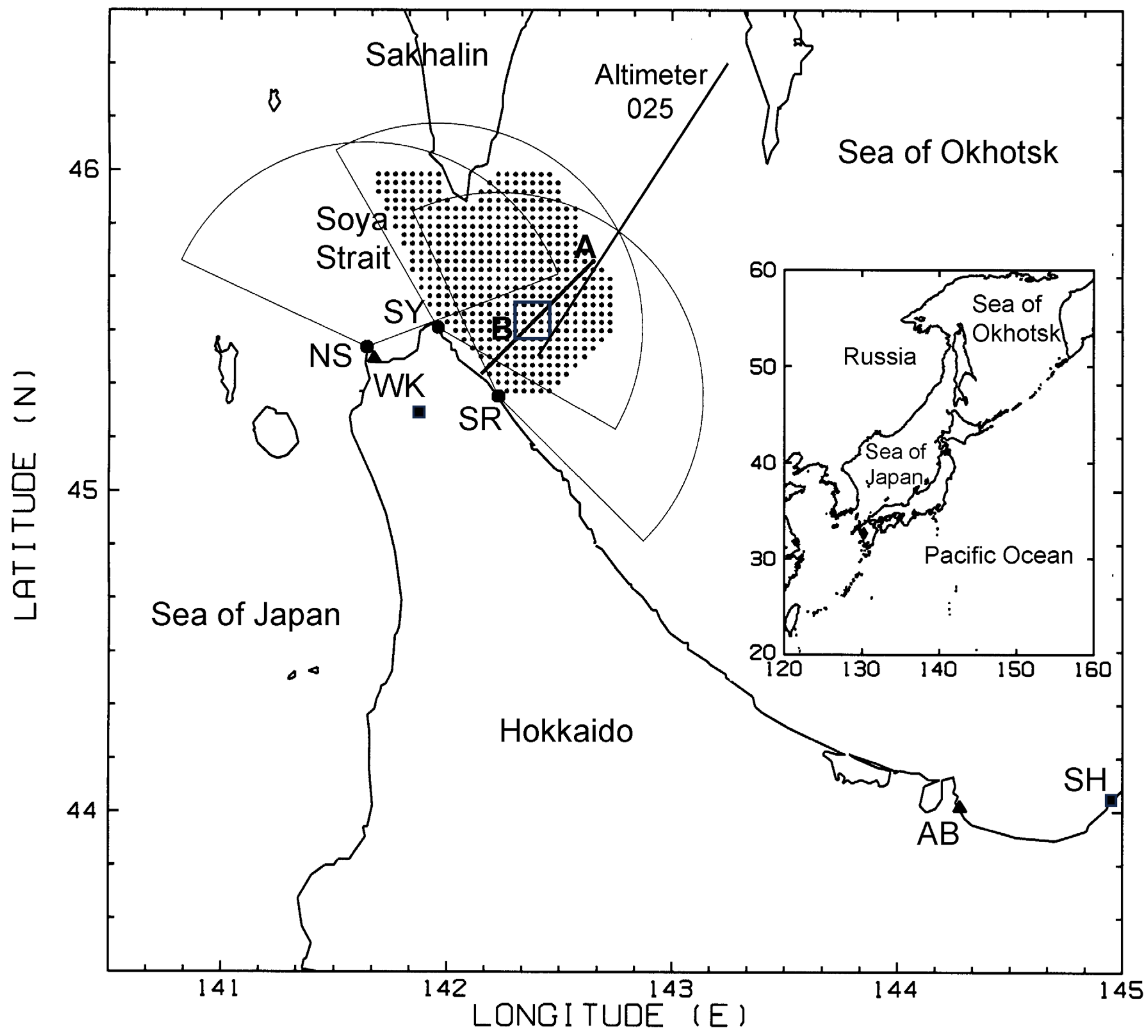

Figure 1. Map of the Soya/La Perouse Strait, location and coverage of the HF radar stations (solid circles, NS: Noshappu radar station, SY: Soya radar station, SR: Sarufutsu radar station), locations of the tide gauge stations (solid triangles, WK: Wakkanai, AB: Abashiri), and GPS stations (solid squares, WK: Wakkanai, SH: Shari). Fans indicate 70 km radii from the HF ocean radar stations and approximate directions of observations. The dots are 3-km grids, where the surface current vectors are composed from the radial velocity components obtained at the HF ocean radar stations. Line A and Box B were used to depict the horizontal alongshore velocity profiles and estimate the alongshore velocity at the SWC axis, respectively. The thin line labeled 025 indicates ground track 025 of satellite altimetry (TOPEX/POSEIODON, Jason-1, -2, and -3).

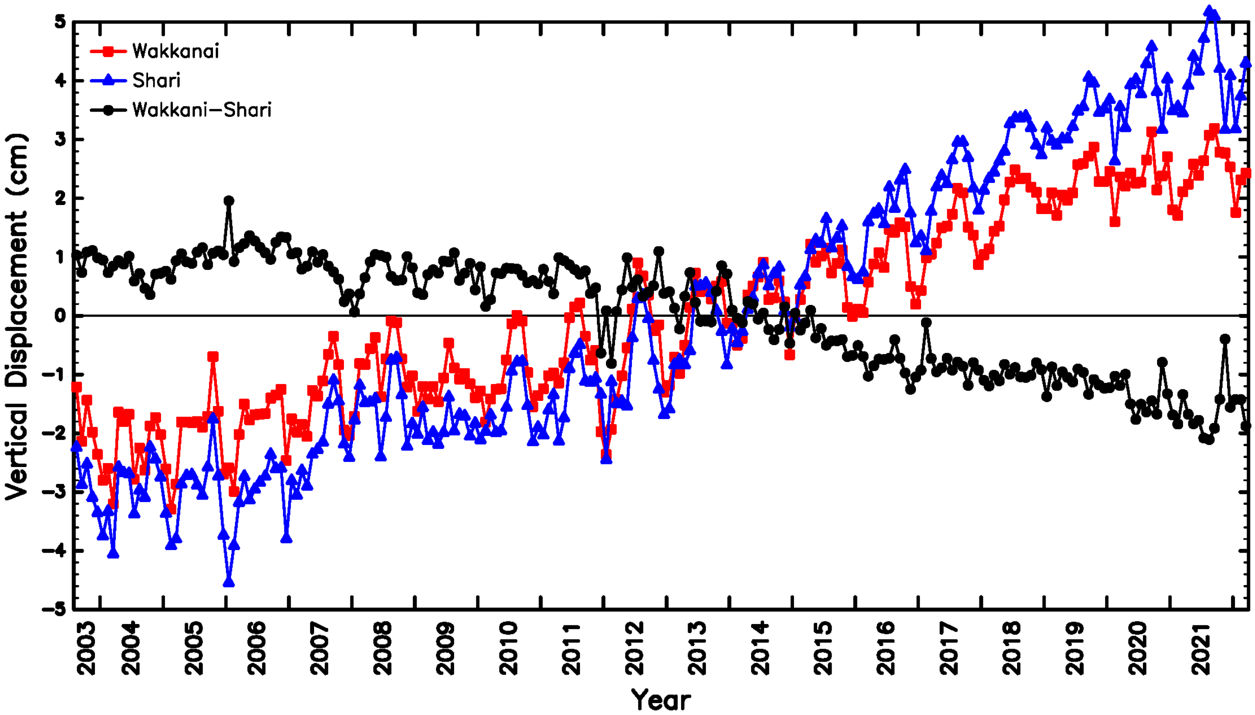

Figure 2. Anomalies of vertical land movements at the GPS stations in Wakkanai (red) and Shari (blue), and the difference between the two stations (black). The average values for the entire study period were subtracted.

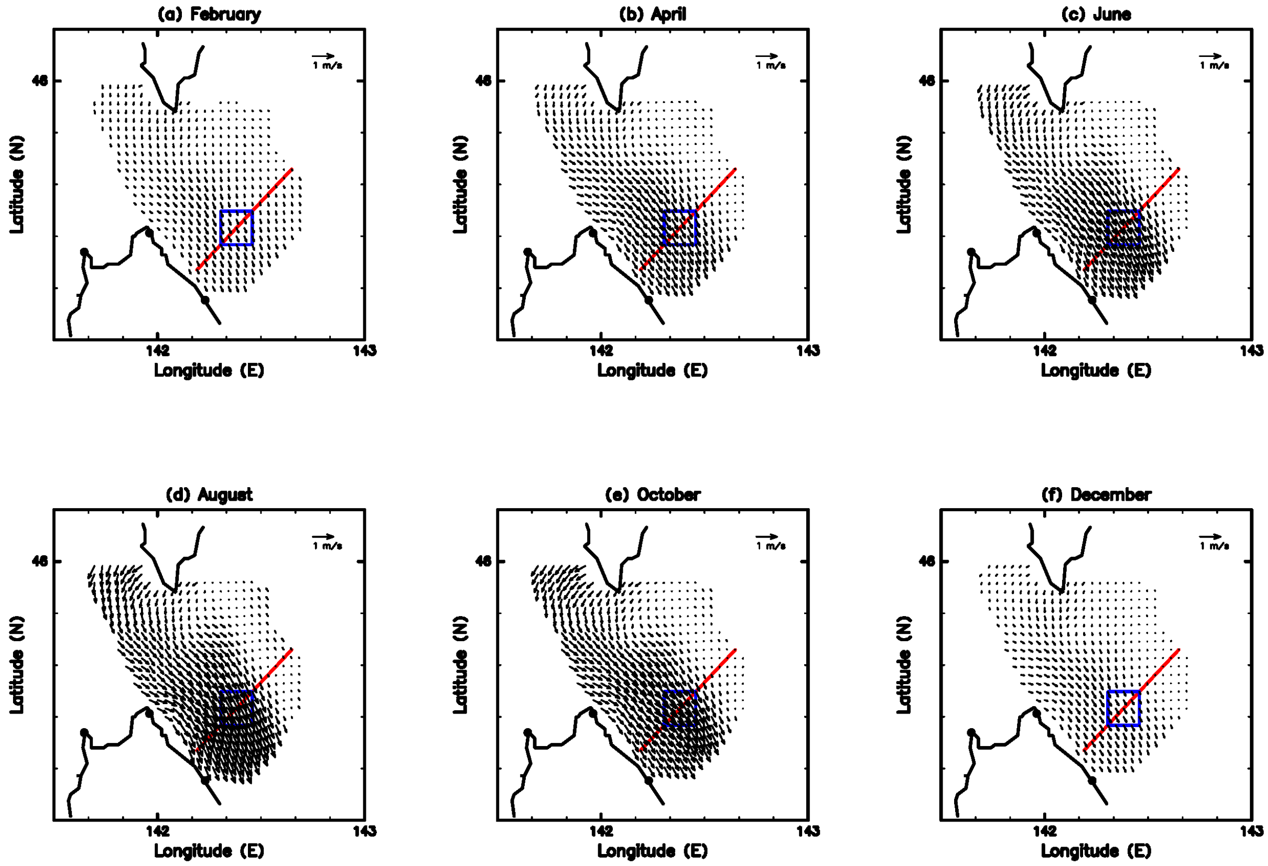

Figure 3. Bi-monthly variations in monthly mean surface current fields. (a) February, (b) April, (c) June, (d) August, (e) October, and (f) December. The locations of Line A and Box B are indicated by red line and blue box. Monthly maps for the full 12 months are shown Online Resource 1.

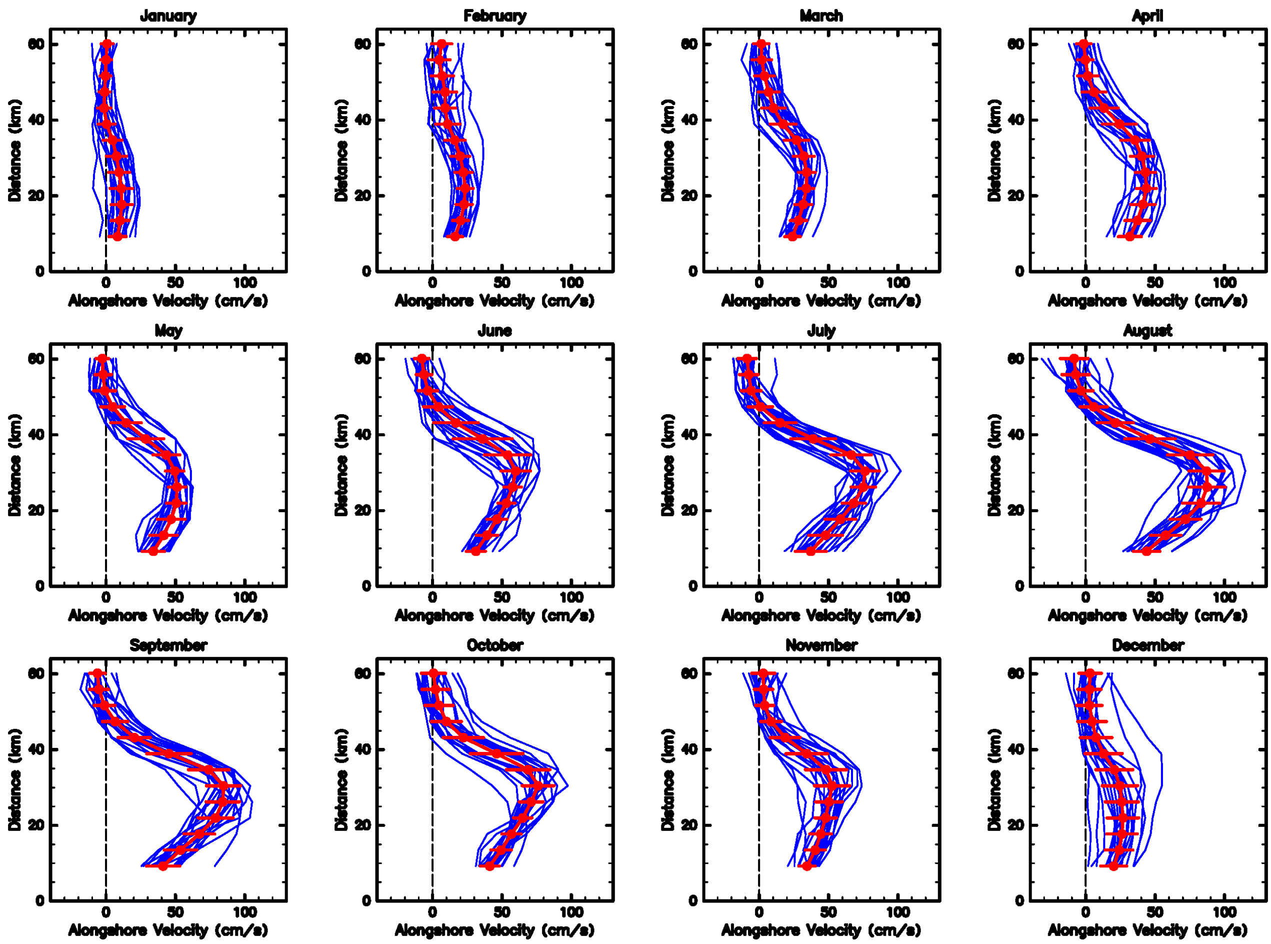

Figure 4. Magnitude of the alongshore velocity component along Line A (Fig. 1) as a function of distance from the coast. The thin blue lines indicate the monthly mean horizontal profile of the alongshore velocity for each year. The thick red lines with error bars indicate the average and standard deviations over the entire observation period.

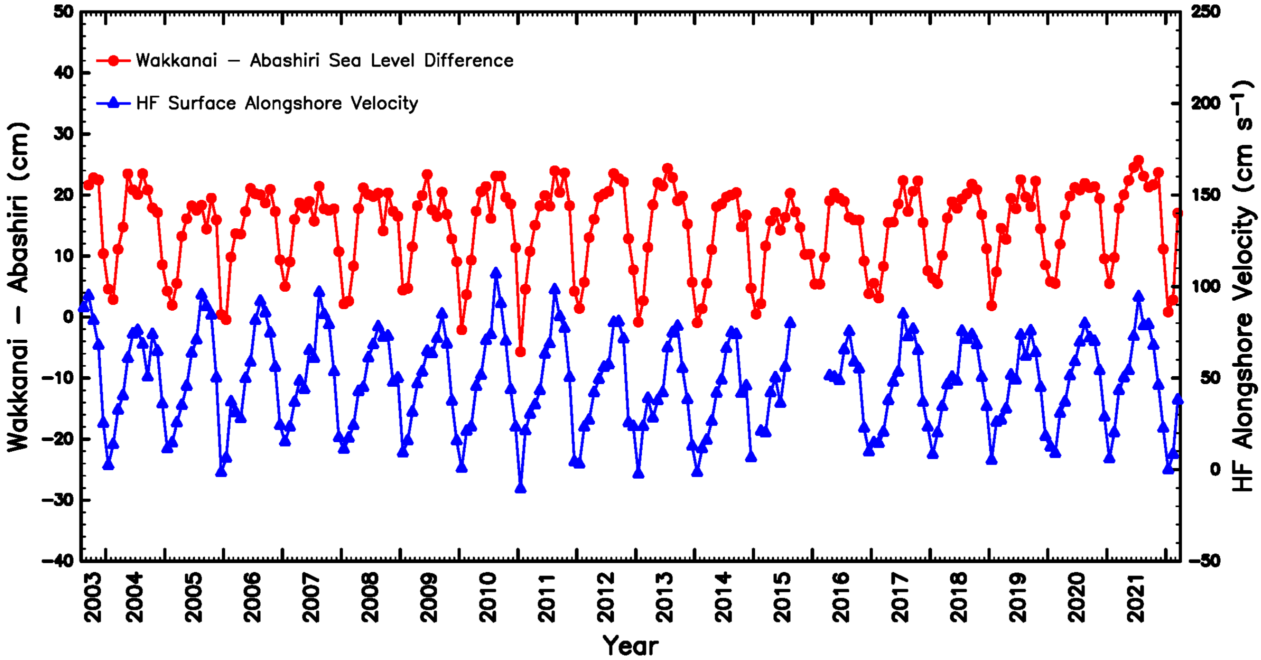

Figure 5. Time series of monthly mean alongshore current velocity in Box B (blue) and alongshore sea level difference between Wakkanai and Abashiri (red).

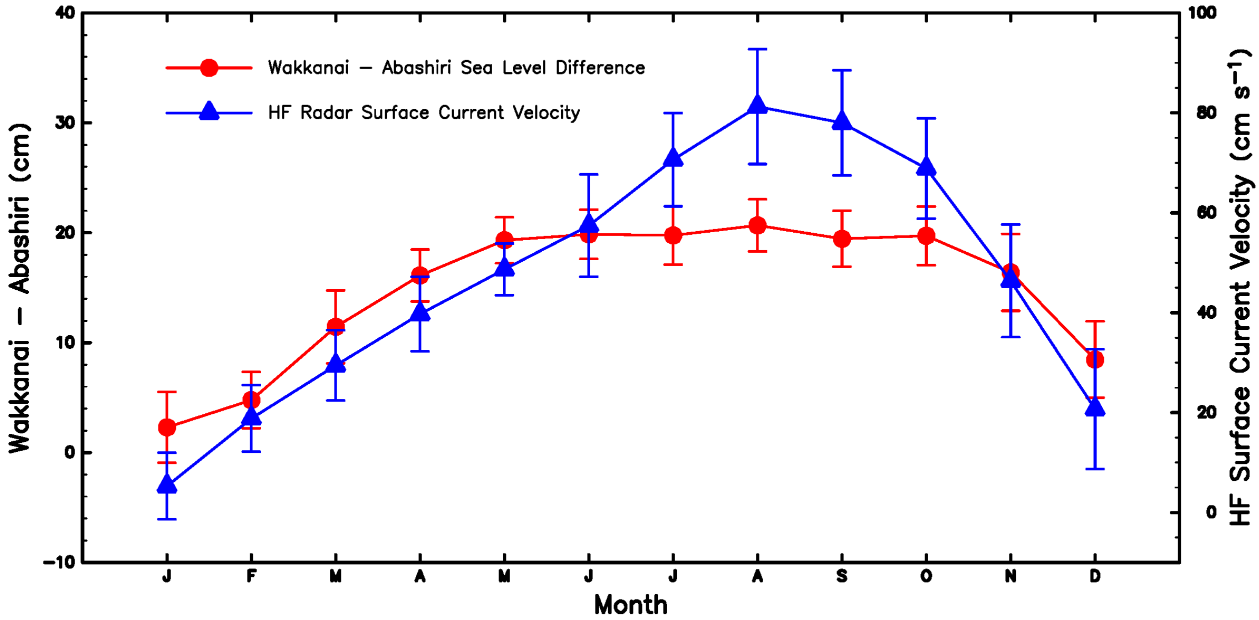

Figure 6. Seasonal variations in the alongshore current velocity in Box B (blue) and the alongshore sea level difference between Wakkanai and Abashiri (red) averaged over the entire observation period. Error bars indicate the standard deviations.

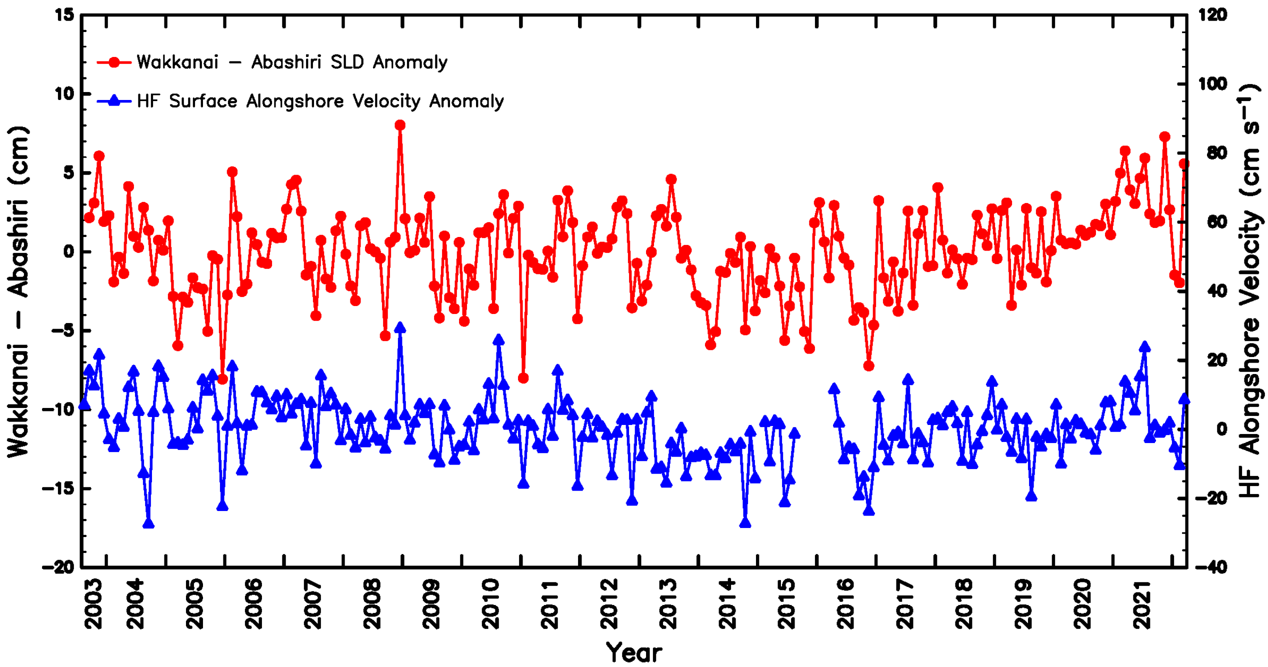

Figure 7. Anomalies of the alongshore current velocity in Box B (blue) and the alongshore sea level difference between Wakkanai and Abashiri (red) from the mean monthly average over the entire observation period.

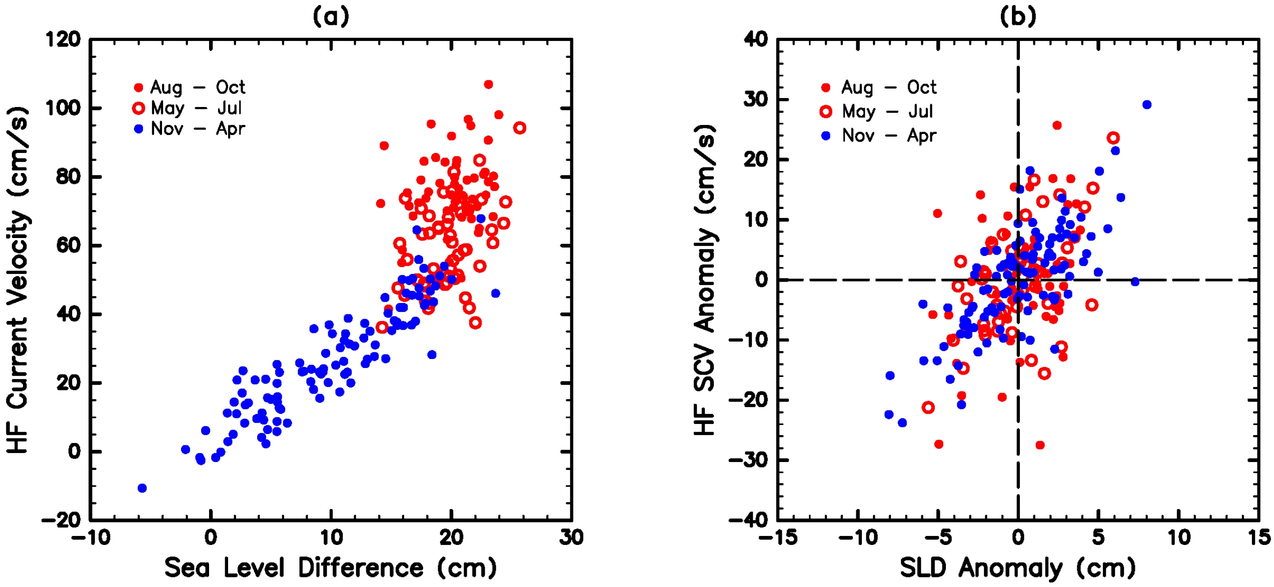

Figure 8. Scatter plots of the alongshore current velocity in Box B and the alongshore sea level difference between Wakkanai and Abashiri (a) with and (b) without seasonal variation. Red open circles, red dots and blue dots indicate the data obtained in May-July, August-October, and November-April, respectively.

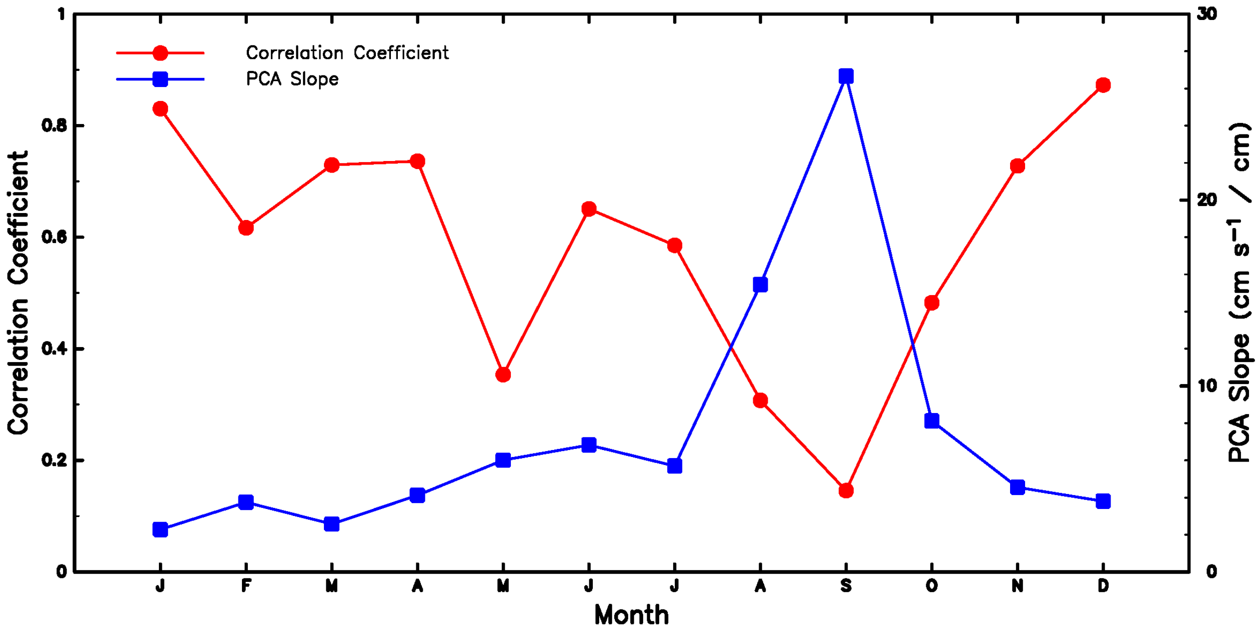

Figure 9. Seasonal variations in the correlation coefficient between the anomalies of the alongshore current velocity in Box B and the alongshore sea level difference between Wakkanai and Abashiri from the mean monthly average over the entire observation period (red). Slopes calculated from the PCA analysis is indicated in blue.

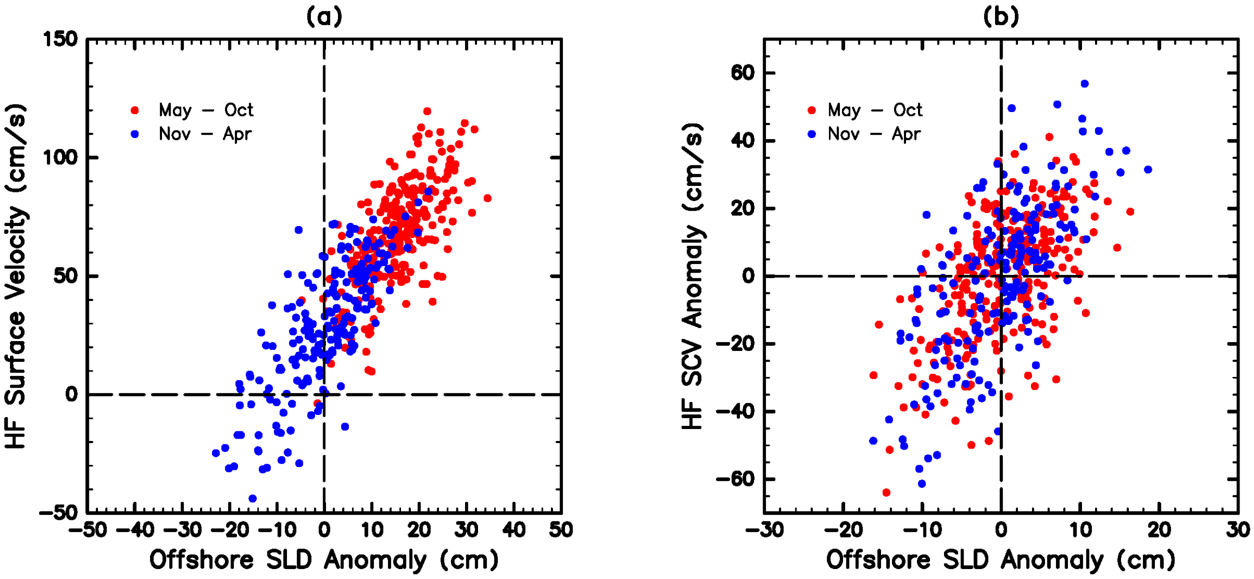

Figure 10 Scatter plots of the offshore sea level difference anomaly estimated using satellite altimetry and coastal tide gauge records at Wakkanai and the HF alongshore surface velocity. (a) Absolute values including seasonal variations, and (b) anomalies from the mean monthly average over the entire observation period. Red and blue dots indicate data obtained in summer (May-October) and winter (November-April), respectively.

Online Resource 1 (Supplementary Information)

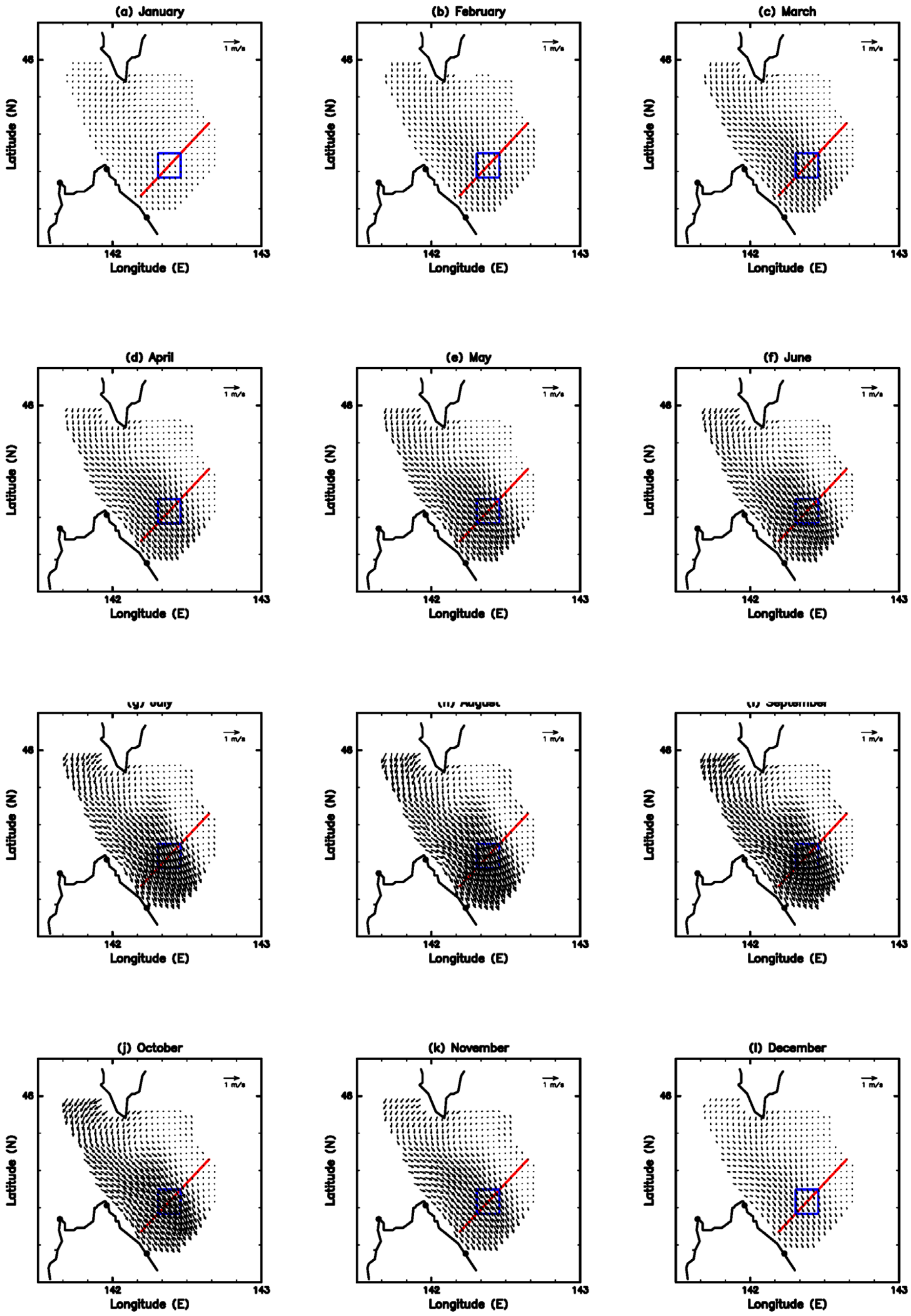

Figure S1. Monthly mean surface current fields from (a) January to (l) December. The locations of Line A and Box B are indicated by red line and blue box.